First-principles predictions: exploring semiconductor properties of $BeXAs_2$ (X=Ge and Sn) for photovoltaic applications

Y. Megdoud[a,b], L. Tairi[b,d], Y. Benkrima[c,*], R. Meneceur[e], A. Lakel[f], S. Ghemid[b], H. Meradji[b], F. Baira[g]
[a]*Institute of Sciences, University Centre of Tipaza, Algeria*
[b]*LPR Laboratory, Département of Physics, Faculty of Science, Badji Mokhtar University, Annaba, Algeria*
[c]*Ecole Normale Supérieure de Ouargla, 30000 Ouargla, Algeria*
[d]*Research Center in Industrial Technologies CRTI, P.O. Box 64, Cheraga16014 Algiers Algeria*
[e]*Unit for the Development of Renewable Energies in Arid Zones (UDERZA), El Oued University, Algeria*
[f]*Material Science Department, Faculty of Science, Biskra University, Biskra 07000, Algeria*
[g]*Department of sciences and technology, Faculty of technology, University of Batna 2, Alleys 53, Constantine Avenue. Fésdis, Batna 05078, Algeria*

In the course of this investigation, we performed ab initio calculations. The investigation systematically explored the physical features of chalcopyrite-phase $BeXAs_2$ (X=Sn and Ge). Total energy calculations incorporated the Wu-Cohen generalized gradient approximation (WC-GGA) [1] to consider the exchange-correlation potential. The analysis of band structures employed the modified Becke Johnson (mBJ) [2] potential approximation, renowned for its effectiveness in addressing concerns related to band gaps. The optical properties of these materials were further elucidated through the determination of the dielectric function and absorption coefficient. The analysis of electronic and optical characteristics underscores the potential applications of $BeXAs_2$ compounds in photonics, optoelectronics, and photovoltaics. Notably, the results exhibit strong agreement with both prior theoretical investigations and experimental data.

(Received April 6, 2024; Accepted July 4, 2024)

Keywords: Materials, Chalcopyrite, FP-LAPW, Bandgap and photovoltaics

1. Introduction

In recent decades, there has been significant interest in chalcopyrite compounds, specifically those falling into the categories in periodic tables (I–III–VI_2 and II-IV-V_2). These materials have garnered attention due to their prominent potential in nonlinear optics, optoelectronics, and electro-optics applications. Their distinct characteristics position them as compelling candidates for a range of applications, including but not limited to solar cells, light-emitting diodes, optical-light eliminators, lasers, photovoltaic detectors, and modulators [3-6]. In the field of optoelectronics, two fundamental aspects hold particular significance: the photoelectric or photovoltaic effect and the emission of light [7]. The ideal material for light emitting diodes or lasers should be a direct band-interdit semiconductor materials with a high oscillation force for direct transitions. The color of the emitted light depends on the band-interdit energy of the material forming P and n type semiconductor (junction). For example, GaP is used in devices operating in the red and infrared spectral regions [8].There is a growing emphasis on photoelectric solar energy converters, given the sun's abundance and reliability as an energy source [5]. For effective photovoltaic cells, a compounds must have a high absorption coefficient and a direct interdit band, preferably close to

* Corresponding author: b-amina1@hotmail.fr
https://doi.org/10.15251/JOR.2024.204.435

1.39 eV, allowing it to absorb light within the VIS (Visible) region [9]. Despite historical challenges related to the exorbitant expenses and suboptimal effectiveness of solar cells, recent research into new materials suitable for photovoltaics, along with advancements in photovoltaic cell fabrication technology, holds promising prospects. Amorphous or crystalline silicon and I–III–VI_2 chalcogenides are among the widely used compounds for cells applications.

In recent years, significant attention has been directed towards I–III–VI_2 chalcogenides, with $CuInSe_2$ standing out due to its approximately 1.0 eV band gap, making it highly efficient in absorbing light [10]. Notably, this compound is commonly employed in thin-film solar cells, often in a solid solution with $CuInSe_2$ (with a interdit band of about 1.7 eV), resulting in solar cell efficiencies of up to 20% [11]. This study focuses on chalcopyrite compounds based on beryllium (Be), specifically $BeGeAs_2$ and $BeSnAs_2$. Notably, there are no experimental studies available for beryllium (Be)-based compounds, and theoretical simulations indicate their potential applications in spintronics devices, particularly when doped with transition elements [12]. All compounds based on beryllium (Be) are thermodynamically stable, as evidenced by their negative enthalpy of formation. Theoretical examinations indicate that $BeGeP_2$ and $BeSnAs_2$ qualify as direct band interdit materials, whereas the remaining four compounds fall into the category of indirect band gap compounds, collectively devoid of magnetic properties.

Several research efforts have contributed to the understanding of these compounds. Shaposhnikov et al. [13] conducted ab-initio calculations on XAZ2 (X = Be, Mg, Zn, Cd; A = Si, Ge, Sn; Z = P, As) ternary tetragonal materials, exploring their electronic, structural, and optical properties. Yu. M. Basalaev, A. V. Kopytov, et al. [14] delved into the modeling of hypothetical $BeXAs_2$ (X = Si, Ge, Sn) crystal structures and phonon spectra. Shah Fahad et al. [15] conducted a comprehensive study on the structural, optoelectronics properties of BeAZ2 (A = Sn; Si, and Ge, Z = As or P) materials.

This paper is structured as follows: A detailed exploration of $BeXAs_2$ ternary compounds (X=Ge and As) is presented, utilizing the Wien2K code [16] within the (DFT) framework [1]. Following this, practical applications of these materials in photovoltaics are systematically discussed. The conclusion in Section 4 summarizes key findings.

2. Theoretical details

This paper employed the augmented and linearized plane waves (FP-LAPW) method [17], implemented within the Wien2k code [16]. This method is a theoretical approach based on the density functional theory (DFT) formalism [1]. Our study primarily focuses on evaluating the physical characteristics of $BeXAs_2$ (X=Ge and Sn) ternary materials. To address the exchange and correlation potential, the Wu-Cohen generalized gradient approximation (WC-GGA) [2] was utilized for optimizing structural parameters. In conjunction with the WC-GGA, the modified Becke-Johnson (mBJ) approximation [3], a recent development, was employed for electronic property calculations. The mBJ method aims to enhance the accuracy of energy gap values, addressing the common underestimation issue encountered with existing approximations. This improvement is particularly crucial for mitigating the shortcomings of DFT [16] in predicting excited states. The method named FP-LAPW [17] involves the partitioning of the computational domain into 2 discrete regions: non-overlapping spheres surrounding the atomic sites, known as Muffin-Tin rays (RMT), and the other region called an interstitial region (IR). In the Muffin-Tin region, the expressions for potentials, basis functions and electron densities integrate a mixture of spherical harmonics up to a specified lmax value (lmax=9 in our study). Conversely, within the interstitial region, these quantities are articulated using Fourier series with a cut-off radius of $R_{MT}K_{max}= 7$, where R_{MT} signifies the smallest radius (In the context of the eigenfunction plane wave expansion, kmax denotes the magnitude of the most substantial wave vector utilized.). The Muffin-Tin radii (RMT) were consistently set at (2.1) value of atomic units for (Ge, Be, As and Sn) atoms, and I, respectively. The energy separation between core and valence states was chosen as -6 Ry. The self-consistent calculations were deemed converged when the E_{Total} demonstrated stability at 0.10 mRy.

3. Results and discussion

3.1. Study of the structural properties

Chalcopyrite materials in the ternary system, specifically denoted as $BeXAs_2$ (where X represents Ge or Sn), showcase a body-centered chalcopyrite (Tetragonal) (bct) crystal phase characterized by (8 atoms) X, with 2 lattice points within each unit cell. The unit cell's spatial coordinates for Be, X, and As are expressed as (0, 0, 0) represent the position of the basic atom, (0, 0,1/2), and Atom 2 as a position (u, 1/4, 0.125), where the internal parameters named (u) serves as the parameter governing anion displacement. In the computational procedure, the energy is determined at various volume values while maintaining a constant c/a ratio. The optimization of the c/a ratio involves calculating the ratio against energy, while the volume is held constant at its minimal value. The minimization of the total energy with respect to the unit cell volume is achieved using Birch-Murnaghan's equation of state [18].

Optimization plots for $BeXAs_2$ (X=Ge and Sn) are depicted in Fig. 1, illustrating the decrease in unit cell energy with volume expansion until reaching a minimum energy state at a specific unit cell volume. Subsequent to this juncture, a discernible upward trajectory in energy is observed. The energy at these minima is designated as the ground state energy (E0(Ry)), and the corresponding volume is identified as the optimal volume. Theoretical determinations encompassing ground state energy, lattice constants a, b and c, internal parameters (u) with the tetragonal distortion named (h=c/(2α)) and the bulk modulus (B_0), the result are organized and presented in (Table 1).

Table 1. Theoretical result of lattice constants (a, c (Å)), c/a ratio, internal parameter u, equilibrium volume V(a.u.)^3 , bulk modulus B_0(GPa) and its first derivative.

Materials		*a*(Å)	*C* (Å)	*C/a*	*u*	V (a.u)^3	B_0(GPa)
$BeGeAs_2$	Present cal	5.38	10.86	2.03	0.22	1062.01	80.61
	Other cal	5.43[a]	10.94[a]	2.012[a]	0.218[a]		
$BeSnAs_2$	Present cal	5.60	11.26	2.01	0.20	1188.2	73.20
	Other cal	5.64[a]	11.36[a]	2.014[a]	0.194[a]		

Ref [a][28].

The rapport (c/a), and the internal parameters (u) closely align with the findings of a previous theoretical study [19]. Additionally, a discernible trend is observed as the values of the equilibrium volume V_0 (in atomic units) increase when progressing from Ge to Sn. Simultaneously, the internal parameter u exhibits a decrease with the transition from Ge to Sn, indicating a structural variation associated with the change in X.

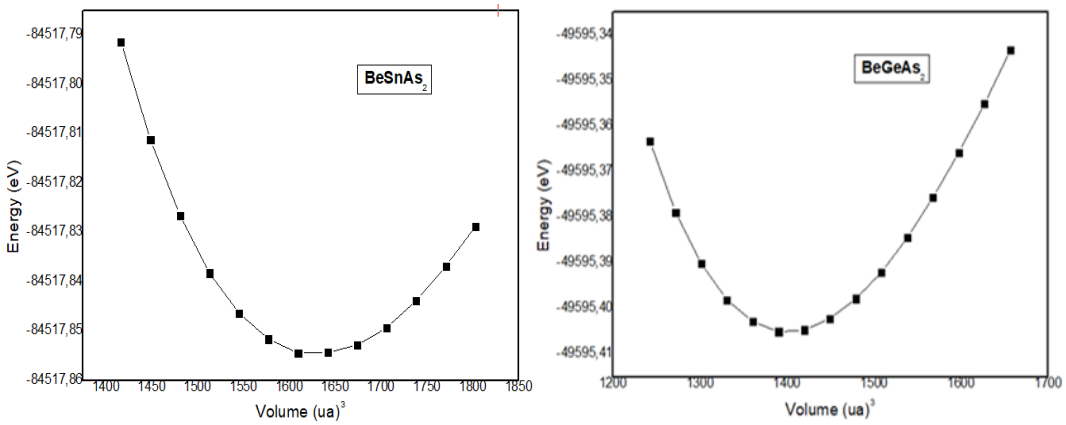

Fig. 1. Total energy versus volume calculated for compounds $BeSnAs_2$ and $BeGeAs_2$.

3.2. Study of the electronic properties

The investigation into the electronic characteristics of Tetragonal compounds $BeXAs_2$ (where X is Ge and Sn) is conducted in a comprehensive manner by analyzing their band structures. Utilizing the mBJ potential, the determined band structures are visually depicted in Fig. 2. It is noteworthy that $BeXAs_2$ (X= Ge and Sn) is identified as a direct band gap material, featuring the difference between of valence band (VB) maxima and conduction band (CB) minima within the same symmetry. This observation aligns with the classification proposed by Shaposhnikov et al. [19], who also recognized these compounds as direct band gap materials.

The result of band gaps, along with additional pertinent data, are summarized in Table 2. A discernible trend is observed: as X transitions from Ge to Sn, there is a systematic increase in band gaps. Notably, the mBJ potential yields superior band gap values compared to the WC-GGA approximation. The agreement of our results with both prior theoretical and experimental data underscores the validity of our findings, further confirming the applicability of these materials in photovoltaic applications.

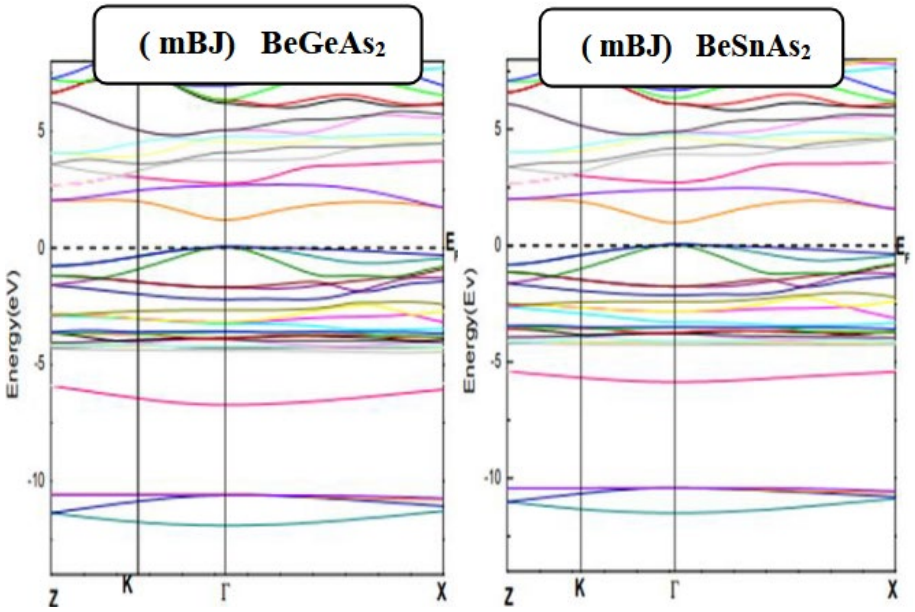

Fig. 2. Calculated band structures of $BeGeAs_2$ and $BeSnAs_2$ compounds using the mBJ approximation.

Table 2. Calculated energy band gap compared with other theoretical values. All energies are in eV.

Materials	WC-GGA	mBJ	mBj	GGA	GW	PLS
	This work		Other work			
$BeGeAs_2$	0.52	1.13	1.15[a]	0.62[a]	1.07[a]	1.68[b]
$BeSnAs_2$	0.73	1.23	1.13[a]	0.68[a]	1.25[a]	1.15[b]

Ref [a][29].

3.3. Study of the optical properties

The microscopic analysis of the interaction between electromagnetic waves and the electrons and ions within a solid is pivotal for comprehending the optical characteristics of solids. The dielectric function, denoted as $\varepsilon(\omega)$, serves as a quantitative macroscopic descriptor of these interactions. Expressed as $\varepsilon(\omega)$, The dielectric function depends on $\varepsilon_2(\omega)$, which is calculated by fundamental electronic transitions. It can also be calculated from the elements of the moment matrix related to the occupied and unoccupied electronic states [20]. The intricately linked polarization

aspect, $\varepsilon_1(\omega)$, actively derives from the imaginary part $\varepsilon_2(\omega)$ through the Kronig –Kramers equation [21,22]. This active relationship establishes a vital connection between the imaginary and real function dielectric components of the dielectric function. Additionally, crucial optical parameters, such as the absorption coefficient $\alpha(\omega)$ and refractive index $n(\omega)$, can be conclude this result deduced from the components of the dielectric function $\varepsilon(\omega)$ using in Kronig-Kramers equation [21,22]. This active macroscopic perspective enables a comprehensive understanding of the dynamic interplay between electromagnetic waves and the underlying electronic and ionic structures within solids.

In our exploration of the optical properties of $BeXAs_2$ (X = Ge, Sn) utilizing the WC-GGA approach, our primary goal is to provide a comprehensive understanding of their relevance in photovoltaic and various optoelectronic applications. These materials exhibit inherent anisotropy, giving rise to two distinct components of the dielectric tensor. One component arises from the electric parallel to the OZ axis for epsilon Z (εz), representing the average spectra of polarizations along the Z directions, while the other is perpendicular to the OZ for epsilon X and Y (εxy).

The Epsilon equation ($\varepsilon = (2\varepsilon\perp c + \varepsilon//c)/3$) [21] governs the determination of the mean result between the insulating components ($\varepsilon\perp c$) with ($\varepsilon//c$). This relationship holds true for other optical parameters as well. Our investigation is centered on elucidating the nuanced optical behavior of these materials, shedding light on their potential applications in the realm of photovoltaics and various optoelectronic devices.

Fig. 3 illustrates the real part of the dielectric function, $\varepsilon_1(\omega)$, for $BeXAs_2$ (X = Ge, Sn) compounds across photon energies up to 30 eV. Notably, both compounds exhibit similar spectra. Analysis of Fig. 3 reveals a shift in the photon energy (E) of the fundamental peak within the visible region (VIS), transitioning from 1.52 eV for $BeGeAs_2$ to 1.37 eV for $BeSnAs_2$. This energy shift is attributed to the electronic band-phases of the materials. The study of photon energy (E) where $\varepsilon_1(\omega)$ is zero in the ultraviolet(UV) region, corresponds not exist of dispersion and signifying to max value of absorption (refer to Figure 4), It saw a decrease from 2.91 to 2.84 eV for $BeGeAs_2$ and $BeSnAs_2$, respectively. Through these energies, the ghost descends below the unit in the ultraviolet until it exceeds the unit in a 16,16 eV for $BeGeAs_2$ and 15.01 eV for $BeSnAs_2$. These frequencies correspond to the plasma frequency (ωp), aligning with the photon energy (E) of the fundamental peak. In the energy range where $\varepsilon_1(\omega) < 0$, electromagnetic waves do not propagate [27], highlighting the critical role of reflectivity in inducing metallic behavior in our compounds.

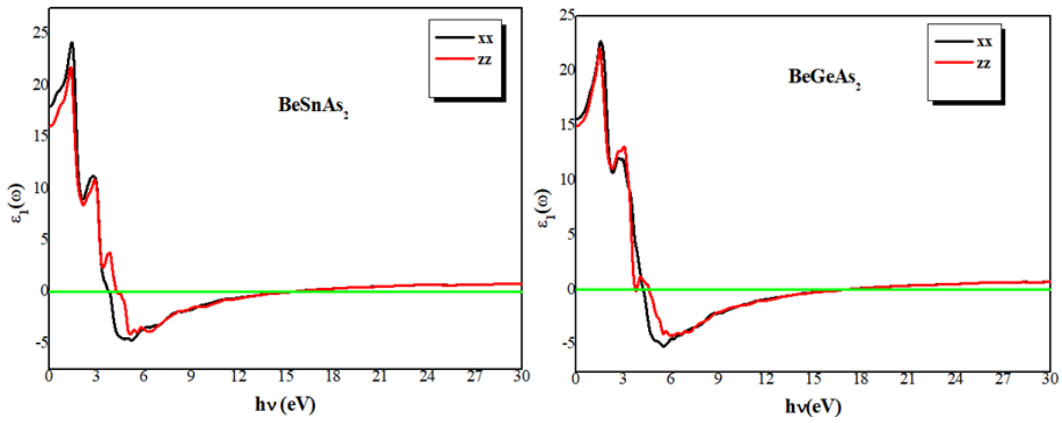

Fig. 3. Calculated real parts of the complex dielectric constant for $BeGeAs_2$ and $BeSnAs_2$ compounds.

The results which are gathered in (Table 3) delineates the static dielectric functions of the studied ternary materials, specifically ($\varepsilon 1(0)\ \perp c$), ($\varepsilon_1(0)//c$), and their average ($\varepsilon_1(0)$), alongside additional theoretical and experimental results.

Table 3. Static Dielectric Function (ε1(0)) and Static Refractive Index (n(0)) Calculations for $BeGeAs_2$ and $BeSnAs_2$ Compounds with mBj method.

Comp	$BeGeAs_2$	$BeSnAs_2$
n(0)	4.981	4.023
$e_1(0)$	15.36	16.87

The absorption-related dielectric function, $\varepsilon_2(\omega)$, is illustrated to 30 eV in Figure 4. It is crucial to emphasize that our optical calculations intentionally exclude indirect band transitions, as the inclusion of phonon scattering in dielectric screening does not significantly impact $\varepsilon_2(\omega)$ [27].

The pivotal energy point in $\varepsilon_2(\omega)$, reflecting the fundamental absorption edge, manifests at approximately 1.68 eV and 1.52 eV for $BeGeAs_2$ and $BeSnAs_2$, respectively. These values are derived using the relation: ($\varepsilon_2 = (2\varepsilon_2 \perp c + \varepsilon_2 // c)/3$) [23]. This optical transition occurs directly at the high point symmetry Γ, involving the minimum result of the valence band (VB) and the maximum value of the conduction band (CB). Consequently, it closely aligns with the bandgap values with mBj method (Figure 4) obtained from this investigated material. These distinctive peaks originate from direct inter-band transitions between various levels within the valence and conduction bands.

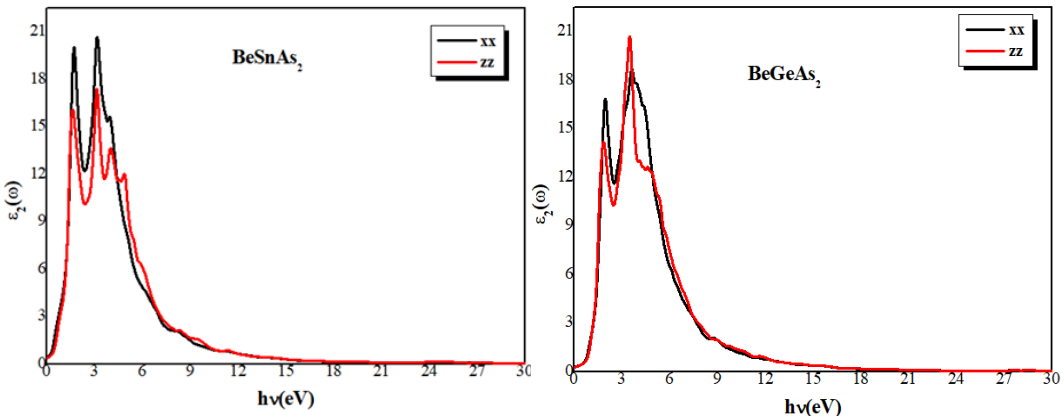

Fig. 4. Computed imaginary parts of the complex dielectric constant for $BeGeAs_2$ and $BeSnAs_2$ compounds.

The dimensionless refractive index, denoted as n(ω), provides a macroscopic representation of the microscopic polarization phenomenon induced by an incident electromagnetic wave and is derived from the values of $\varepsilon_1(\omega)$ and $\varepsilon_2(\omega)$ [23]. The refractive indices for the materials of interest are depicted in Figure 5, illustrating that n(ω) exhibits the same isotropic property as $\varepsilon_1(\omega)$.

The static refractive index values, determined through the relationship n (0) = sqrt ($\varepsilon_1(0)$), closely correspond with those directly obtained from the refractive index plots, measuring 3.92 and 4.20 for $BeGeAs_2$ and $BeSnAs_2$, respectively (refer to Table 3). Notably, Table 3 delineates an elevation in static result from $BeGeAs_2$ to $BeSnAs_2$, consistent with the increase in this value. This escalation is attributed to the diminishing Energy gap, inversely correlating with ε1(0) and consequently with n(0).

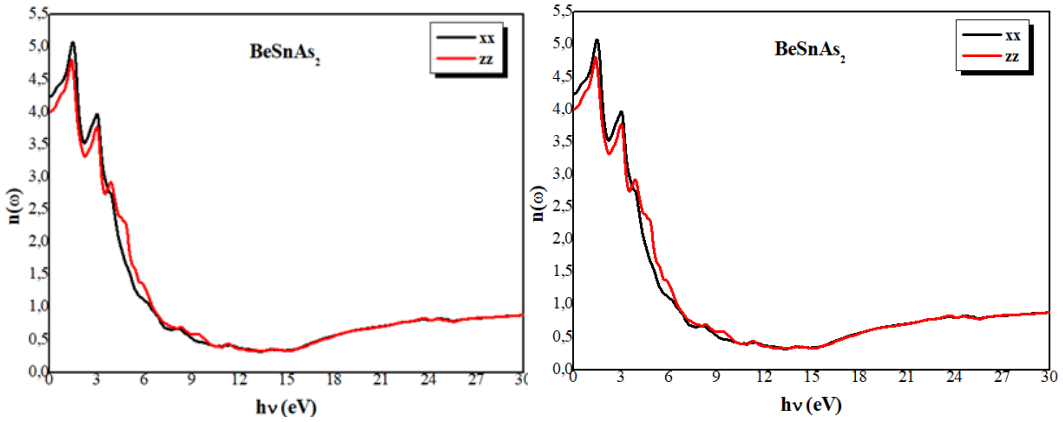

Fig. 5. Variation of refractive index n(ω) for $BeGeAs_2$ and $BeSnAs_2$ compounds.

The intrinsic anisotropy inherent in chalcopyrite compounds, leading to birefringence, emerges as a notable advantage. Birefringence confers exceptional nonlinear optical properties to our investigated compounds, facilitating phase adaptation through angular adjustments achieved by simply rotating the crystal relative to the incident beam [24-25]. These distinctive characteristics position our compounds favorably for applications [26-27].

Absorption spectra for varying concentrations are depicted in Fig. 6, illustrating that absorption occurs exclusively when photon energy surpasses the band gap. This phenomenon is attributed to the excitation of electrons in the (VB) to the (CB). The influence of polarization on the spectrum is observed to be minimal.

In Fig. 6, the absorption edge is identified at 1.16 eV and 0.22 eV for $BeGeAs_2$ and $BeSnAs_2$, respectively, aligning with the band gap values evaluated at these concentrations. Beyond these energy values, the absorption coefficient experiences an increase, reaching a maximum at a specific energy before gradually decreasing with slight oscillations. The variation in the absorption edge concerning concentration is ascribed to a reduction in the band gap. Across all considered concentrations, the absorption coefficients exhibit a rapid decline in the low-energy region, characteristic of semiconductor behavior.

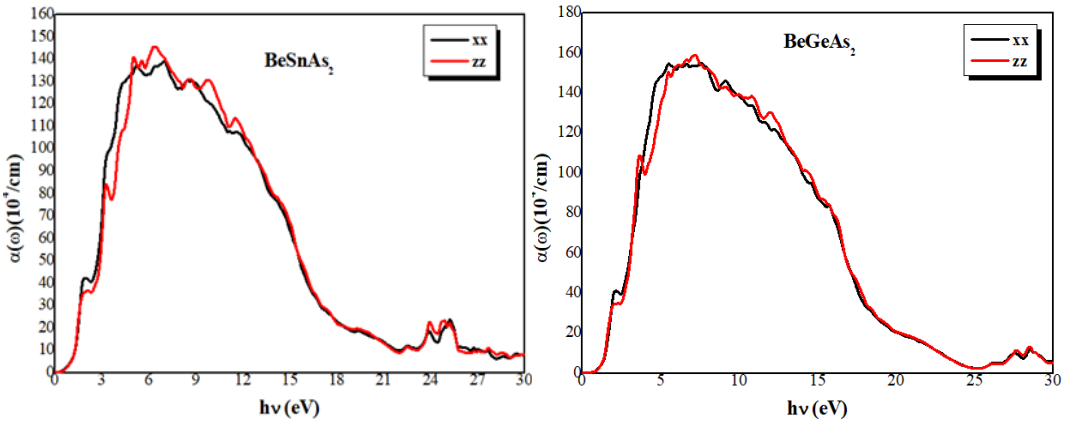

Fig. 6. Calculated absorption coefficient α(ω) versus energy (eV) for $BeGeAs_2$ and $BeSnAs_2$ compounds.

The evolution of reflectivity for the examined compounds is portrayed in Figure 7, illustrating the spectra of reflectivity values within the energy range [0-30] eV. The curves indicate a maximum of 35% for $BeGeAs_2$ and 38% for $BeSnAs_2$. These results underscore the suitability of our materials for application in the infrared domain, as reflected by their substantial reflectivity.

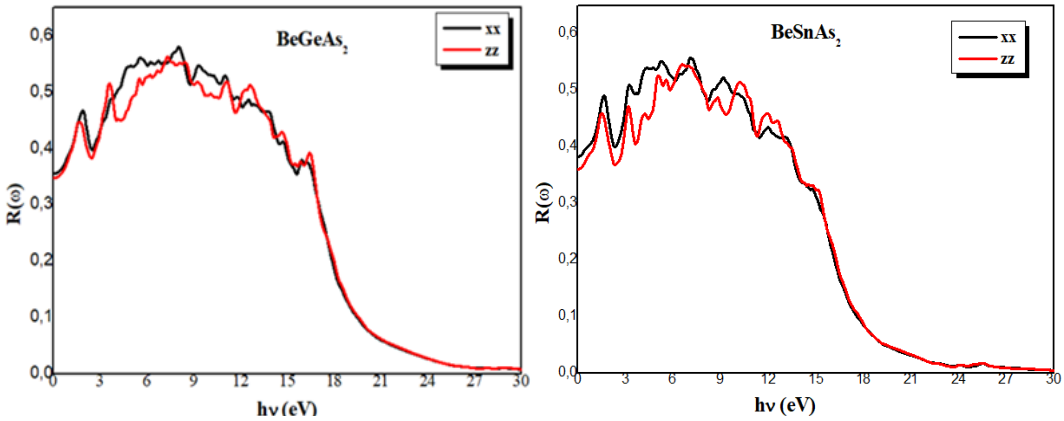

Fig. 7. Reflectivity (R(ω)) variation for for $BeGeAs_2$ and $BeSnAs_2$ compounds.

4. Conclusion

In this paper, a comprehensive analysis of the ternary alloys $BeGeAs_2$ and $BeSnAs_2$ was undertaken through first-principle calculations utilizing (FP-LAPW) method within the framework of DFT theory. The results of this rigorous examination reveal the notable potential of these compounds in the realms of photonics and photovoltaics. Comparative assessments of calculated lattice constants and band-gap values against existing theoretical and experimental data substantiate the favorable characteristics of $BeGeAs_2$ and $BeSnAs_2$ for these pivotal applications. Furthermore, the study delves into the optical properties, encompassing the dielectric function, reflectivity, refractive index, and absorption coefficient, elucidating nuanced aspects of these materials.

These findings not only contribute valuable insights into the properties of $BeGeAs_2$ and $BeSnAs_2$ but also pave the way for further advancements in materials science. The demonstrated potential of these alloys holds promise for the progression of innovative photonic and photovoltaic technologies. This study represents a significant advancement in materials science, underscoring the intricacies of scientific inquiry. By leveraging advanced computational methods, researchers can unlock the full potential of materials such as $BeGeAs_2$ and $BeSnAs_2$, propelling the field into a new era of exploration and advancement.

References

[1] Z. Wu, R.E. Cohen, Phys. Rev. B 73, 235116 (2006); https://doi.org/10.1103/PhysRevB.73.235116.
[2] Tran F, Blaha P. Phys Rev Lett.; 102 226401–226405 (2009); https://doi.org/10.1103/PhysRevLett.102.226401
[3] E. Rosencher, B.Vinter, (Cambridge University Press, Cambridge, UK, (2002). doi: https://doi.org/10.1017/CBO9780511754647
[4] C. Rincón, C. Bellabarba, J. González, G. Sánchez Pérez, Materials Science, Physics Solar Cells, 16, 335-349 (1986) Doi; https://doi.org/10.1016/0379-6787(86)90093-1.
[5] J.L. Shay, L.M. Schiavone, E. Buehier, J.H. Wernick, J. Appl. Phys. 43, 2805 (1972). Doi: https://doi.org/10.1063/1.1661599
[6] H. Horinaka, S. Mononobe, N. Yamamoto, Jpn. J. Appl. Phys. 32, 109 (1993). Doi: http://dx.doi.org/10.7567/JJAPS.32S3.109
[7] E. Rosencher, B. Vinter, Optoelectronics, Cambridge University Press, Cambridge, UK, (2002).Doi: https://doi.org/10.1017/CBO9780511754647
[8] W.N. Shafarman, L. Stolt, in A. Luque, S. Hegedus (Eds.)
[9] J.E. Jaffe, A. Zunger, Phys. Rev. B29, 1882 (1984); https://doi.org/10.4236/wjcmp.2014.44027

[10] A.V. Krivosheeva, V.L. Shaposhnikov, F. Arnaudd'Avitaya, V.E. Borisenko, J.- L. Lazzari, J. Phys, Condens. Matter. 21, 045507 (2009). Doi: http://dx.doi.org/10.1002/chin.201541001
[11] W. N. Shafarman and L. Stolt, in Handbook of Photovoltaic Science and Engineering, edited by A. Luque, S. Hegedus (Wiley, Chichester, UK, pp. 567–616 (2003).doi: https://doi.org/10.1016/j.cocom.2016.09.001
[12] M. A. Green, K. Emery, Y. Hishikawa, W. Warta, Prog. Photovolt: Res. Appl. 18, 346 (2010).doi: https://doi.org/10.1002/pip.1021
[13] A V Krivosheeva, V L Shaposhnikov, F Arnaud D'Avitaya, V E Borisenko and J-L Lazzari, Journal of Physics: Condensed Matter, 21, 045507 (2009); https://doi.org/10.1088/0953-8984/21/4/045507
[14] Yu. M. Basalaev, A. V. Kopytov, et al, Russian Physics Journal, 126651312 (2019). Doi: https://doi.org/10.1103/PhysRevB.85.205201
[15]Shah Fahad, G. Murtaza, T. Ouahrani, R. Khenata, Masood Yousaf, S.Bin Omran, Saleh Mohammad, Journal of Alloys and Compounds, 646, 211-222 (2015).doi: https://doi.org/10.1016/j.jallcom.2015.06.026
[16] Blaha P, Schwarz K, Madsen GKH, et al. WIEN2K, Vienna; (2008); https://doi.org/10.1103/PhysRevB.12.3060
[17] Hohenberg P, Kohn W. Phys Rev. 136, 864–871 (1964); https://doi.org/10.1103/PhysRev.136.B864
[18] F.D. Murnaghan, Proc. Natl.Acad.Sci.U.S.A. 30, 5390 (1944); https://doi.org/10.1103/PhysRev.140.A1133
[19] V.L. Shaposhnikov, A.V. Krivosheeva, V.E. Borisenko, J.L. Lazzari, F.A. d'Avitaya, Phys. Rev. B 85 20520 (2012); https://doi.org/10.1103/PhysRevB.73.235116
[20] J. S. Toll, Causality and the Dispersion Relation: Logical Foundations, Phys. Rev. 104, 1760 (1956); https://doi.org/10.1103/PhysRev.104.1760
[21] L. D. Landau, E. M. Lifshitz, Electrodynamics of Continuous Media (Pergamon Press, Oxford, 1960).
[22] H. A. Kramers, Collected Science Papers (North-Holland Publishing Co, Amsterdam, 1956)
[23] R. de. L. Kronig, J. Opt. Soc. Am. 12, 547 (1926); https://doi.org/10.1364/JOSA.12.000547
[24] C. M. I. Okoye, J. Phys. 15, 5945 (2003) ; https://doi.org/10.1088/0953-8984/15/35/304
[25] P. Y. Yu, M. Cardona, Fundamentals of Semiconductors (Springer-Verlag, Berlin, 1996)
[26] A. H. Reshak et al. Alloys Compd. 509, 6737 (2011); https://doi.org/10.1016/j.jallcom.2011.03.029
[27] C. S. Schnohr, AIP, Appl. Phys. Rev. 2, 031304 (2015)
[28] V.L. Shaposhnikov, A.V. Krivosheeva, V.E. Borisenko, J.L. Lazzari, F.A. d'Avitaya, Phys. Rev. B 85, 20520 (2012)
[29] R. Mahdjoubi, Y. Megdoud, L. Tairi, H. Meradji, Z. Chouahda, S. Ghemid, F. El Haj Hassan. International Journal of Modern Physics B, (2019)